Celestial Mechanics and Dynamical Astronomy manuscript No.
(will be inserted by the editor)

A Multiresolution Model for Small-Body Gravity Estimation

Brandon A. Jones · Gregory Beylkin ·
George H. Born · Robert S. Provence

Received: date / Accepted: date

Abstract A new model, dubbed the MRQSphere, provides a multiresolution representation of the gravity field designed for its estimation. The multiresolution representation uses an approximation via Gaussians of the solution of the Laplace's equation in the exterior of a sphere. Also, instead of the spherical harmonics, variations in the angular variables are modeled by a set of functions constructed using quadratures for the sphere invariant under the icosahedral group. When combined,

addition, instead of the spherical harmonics, we model variations in the angular directions by an alternate set of functions constructed using quadratures for the sphere invariant under the icosahedral group. This paper presents an initial proof of concept to unweave the estimation problem from its current reliance on the spherical harmonics and the expansion of the gravity potential via the inverse powers of the radial variable.

When estimating the gravity field of a primary body, it is important to stage the estimation in a natural manner. In such a procedure, one would like to first obtain the low spatial frequencies of the model and, then, gradually higher spatial frequencies as we approach the body. The classical representation of the gravity potential via the inverse powers of the radial variable is ill-suited for such an

problems for using the spherical harmonics models. As seen in Fig. 1 (generated from NEAR laser range nder results (Zuber et al, 2000)), the asteroid 433 Eros is roughly ellipsoidal in shape. For this reason, the ellipsoidal harmonics model is more appropriate than the spherical one. Results indeed demonstrate the advantages of the ellipsoidal harmonics gravity model (Garmier et al, 2002). For both the spherical and ellipsoidal harmonics models, the partial sum diverges for points within the circumscribing sphere (or ellipsoid), thus limiting the minimum valid altitude. Unfortunately, not all asteroids are ellipsoidal and, thus, other gravity representations suited for a more-or-less arbitrary shape are desired.

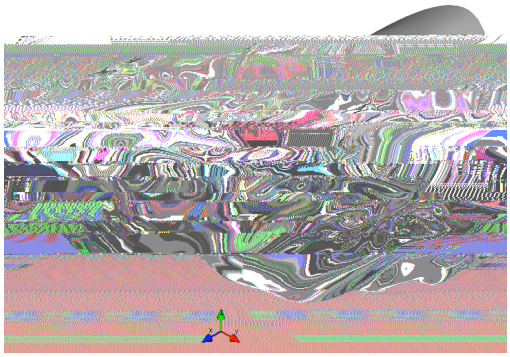

Fig. 1 An isometric view of the asteroid 433 Eros.

The goals of this paper are to introduce the new model and demonstrate its estimation capabilities. We accomplish this by applying the model to the asteroid 433 Eros, using the NEAR15A gravity model (Konopliv et al, 2002) derived from observations of the NEAR satellite. We start by presenting the MultiResolution representation and Quadratures for the Sphere (MRQSphere) model. This includes a description of the mathematical tools employed in de ning the model, and their combination to create the model, and the speci c choice of model parameters used in the paper. We then de ne the estimation method and present results from a simulation study. Finally, we provide conclusions and describe additional work required for its practical implementation.

2 MRQSphere Model

The MRQSphere model combines two recently developed mathematical tools to provide a multiresolution representation of the gravity eld, i.e. a model with a resolution that varies with altitude. One of these tools approximates the radial decay of the gravity eld using a sum of Gaussians, while the second one employs interpolation on the sphere to represent the angular variations. Using these tools, we evaluate a function on each one of a collection of spheres, or shells, and combine

where

$$V_n(\ ;\ ) = \sum_{m=0}^{\infty} P_{n;m}[\sin\ ](C_{n;m}\cos m\ + S_{n;m}\sin m\ ): \tag{3}$$

Instead of using the representation in Eq. 3, we want to represent V_n using its values on the sphere. For this purpose, we use the reproducing kernel (see Ahrens and Beylkin (2009)). Let P_N be the space of spherical harmonics of maximum degree and order N. The reproducing kernel

$$K_N(\ \ ^0) \sum_{n=0}^{N} \frac{2n+1}{4} P_{n;0}(\ \ ^0); \tag{4}$$

has the property that for any function f in P_N, we have

$$f(\ ) = \int_{S^2} K_N(\ \ ^0) f(\ f(\text{n Eq.}$$

f

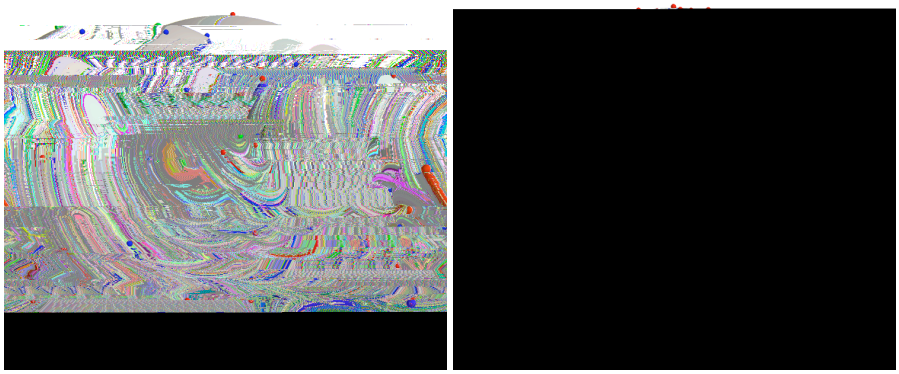

(a) 2N=14, 72 Points (b) 2N=30, 372 Points

Fig. 2 Sample quadratures for the sphere for di erent degree models

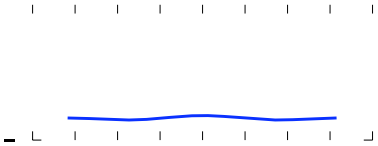

Fig. 3 Sample plots of the reproducing kernel K_N as a function of the angle between the vectors and ^{0} for various degrees N

where $P_N^{(1;0)}$ is the Jacobi polynomial with =1 and =0. To simplify notation and prevent confusion of $P_N^{(1;0)}$ with the Legendre polynomials P_N, we denote

$$K_N( ) = P_N^{(1;0)}( ) = \frac{4}{N+1} K_N( ): \tag{9}$$

In our approach we estimate functions $Z_j(\ )$ directly, thus avoiding any use of the spherical harmonics when evaluating the model. This Cartesian representation also eliminates any singularity at the poles when evaluating the acceleration. We note that, for a given accuracy, the exponential cuto in Equation 22 allows us to predict the degree of the subspace of spherical harmonics for the functions Z_j and, thus, choose the appropriate number of quadrature nodes for estimation. We also note that, as described in Beylkin and Monzon (2010), the number of terms in Equation (21) depends only weakly on the required resolution and is relatively small. For a xed , only a few terms in Equation (21) contribute to the potential.

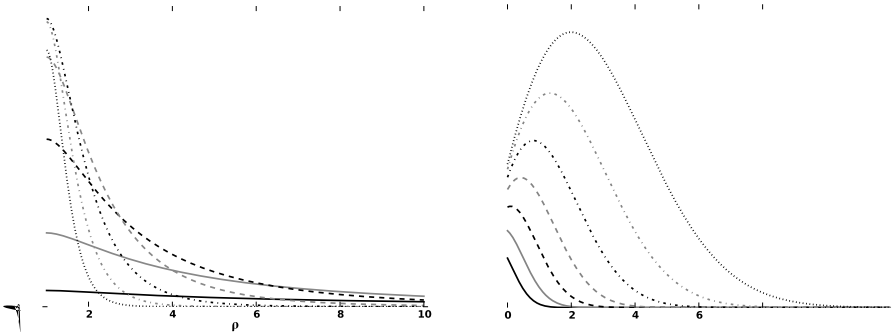

(a) Shell contributions ($n=2$) (b) Shell degree contribution

Fig. 5 The rst gure illustrates the contributions of the di erent shells to the function $G_{h;\mathrm{J}}$ (h = 0:5) with variations in orbit radius (in units of R_E), while the second gure demonstrates the contribution of gravity degree n for a given shell

In Fig. 5, we plot the terms of the series in Eqs. 19 and 22 with h = 0:5. As

Table 2 Shells required at given radii (accurate to 10 ^{5})

Range (in R_E)	J_{min}	J_{max}
Above 33.963085	-5	0
33.963085 - 17.221399	-5	1
17.221399 - 10.223156	-5	2
10.223156 - 6.437202	-5	3
6.437202 - 4.578281	-5	4
4.578281 - 3.412891	-5	5
3.412891 - 2.702480	-5	6
2.702480 - 2.244688	-5	7
2.244688 - 1.925941	-5	8

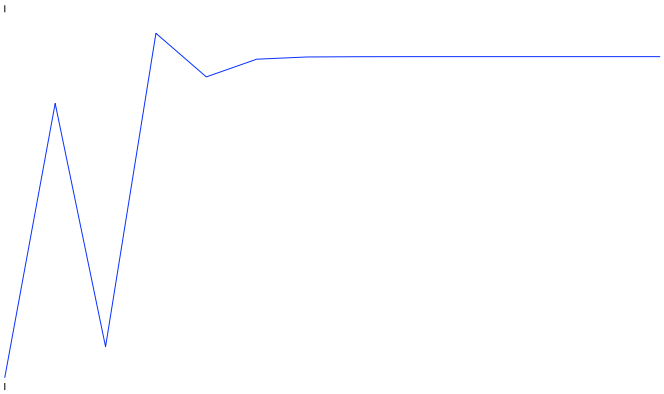

Fig. 6 Precision (in units of 10 ^{10}) of the approximation by Gaussians of $^{(n+1)}$ using shells -5 through 1 at a radius of 17.2214 R_E

In Fig. 6 we illustrate the precision of approximating $^{(n+1)}$ using Gaussians with the parameters shown in Table 1. We see in this gure that, unlike at the other altitude ranges listed in Table 2, the corresponding shells at slightly above the radius 17.221399 barely meet the precision requirement of 5 10 ^{10}. This in uences future results, speci cally, the precision of the MRQSphere model as the radius of decreases towards 17.22 R_E. The upper boundary for including shell 2 may be changed to avoid this phenomenon but we have not done so intentionally

With the subset J now speci ed, the shell degrees, and thus the number of quadrature nodes required, may be determined. We select the number of terms in Z_j to achieve a relative accuracy of 7 signi cant digits and provide the resulting values in Table 3. Quadratures on the sphere are currently available only for particular degrees, thus for a given j we use the minimal number of nodes that guarantees proper integration. We denote the corresponding degree as n_{max}. Additionally, we place a limit of degree 15 on the shells given that the NEAR15A model is 15 15.

Table 3 Required gravity field degree (n_{max}) and the number of quadrature nodes for each shell

$j-J$	n_{max}	M	$j-J$	n_{max}	M
-5	4	32	2	14	312
-4	4	32	3	15	372
-3	4	32	4	15	372
-2	7	72	5	15	372
-1	7	72	6	15	372
0	9	132	7	15	372
1	11	192	8	15	372

2.5 Baseline Performance

To provide a basis of comparison, and gain a more thorough understanding of the ideal performance of the MRQSphere model used for this study, we perform a set

A comparison of the MRQSphere model accelerations with those of the spherical harmonics model is provided in Fig. 7. As the radius decreases, the precision improves. For a xed , which controls the approximation via Gaussians, the number of accurate digits in Eq. 19 increases for lower altitudes. As the radius decreases towards 17 R_E

Fig. 9 Relative accuracy of the Laplacian ($r^2 \nabla$) of the idealized MRQSphere model when compared to the maximum diagonal element of the variational equation matrix, with the gure on the right illustrating the distribution of signi cant digits with radius

Fig. 10

Fig. 11 Summary of 3D RMS orbit propagation errors using the baseline MRQSphere model for Eros.

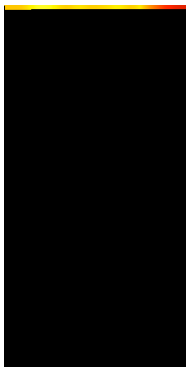

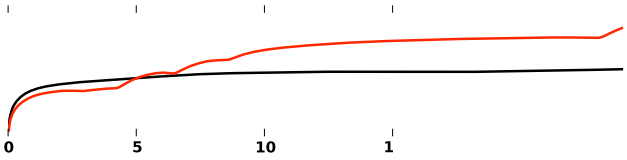

Fig. 13

Sphere model. We note that equatorial orbits within approximately 2 R_E in radius correspond to the regions of instability derived in Scheeres (2002).

where the $r \times r$ matrix S^0 contains the non-zero singular values and r is the numeric rank of H. We assume that singular values below a certain threshold are set equal to zero. The pseudoinverse of H is calculated using SVD, and solutions of Eq. 29 may be expressed as

$$\hat{x} = V \begin{bmatrix} S^{0\ -1} & 0 \\ 0 & 0 \end{bmatrix} W^T y. \tag{34}$$

For the weighted least squares using SVD, the solution is written as

$$\hat{x} = V \begin{bmatrix} S^{0\ -1} & 0 \\ 0 & 0 \end{bmatrix} W^T \sqrt{B^{-1}}\, y, \tag{35}$$

where

$$\sqrt{B^{-1}} H = V^T S W. \tag{36}$$

The state-error covariance matrix, $E[(\hat{x} - x)(\hat{x} - x)^T]$, where x is the true state, provides some statistical information on the quality of the solution $\hat{x}$. In the case of the least-squares algorithm with SVD, it may be shown that (e.g., see Ahn, 1996)

$$E[(\hat{x} - x)(\hat{x} - x)^T] = V \begin{bmatrix} S^{0\ -2} & 0 \\ 0 & 0 \end{bmatrix} V^T. \tag{37}$$

3.2 Estimation Process

Missions to bodies beyond Earth orbit often utilize a statistical filter, usually a square-root information filter (SRIF), to estimate the satellite position, gravity field, and other parameters using radio science and other observations available. To simplify the gravity recovery process for this proof of concept, we only estimate the terms of the gravity field. We assume the satellite state is known, with measurements of the gravity potential provided with some accuracy. Furthermore, we only estimate the Z_j values for a single shell at a time as we approach the asteroid. Thus, our estimated state vector is

$$X_j = \begin{bmatrix} \sqrt{w_1} Z_j(\ _1) \\ \sqrt{w_2} Z_j(\ _2) \\ \vdots \\ \sqrt{w_M} Z_j(\ _M) \end{bmatrix} \tag{38}$$

where M is the number of nodes for a given shell. The reason for the $\sqrt{w_j}$ factor will be explained later.

MRQSphere model starts with the initial range of shells -5 through -1, we must assume an a priori estimate of these shells is available. Section 3.4 discusses how this may be accomplished.

gravity field. We note that these trajectories are independent of those used in the orbit propagation tests of Section 2.5. Using the NEAR15A model, we evaluate the potential at points on these orbits to generate the observations U_i. Nine sets of observations are generated, one each for the range of orbit radii in Table 2. Thus we have one set of observations for each of the shells indexed from 0 through 8. We propagate orbits long enough to provide (roughly) complete coverage of the gravity field, i.e. groundtracks overlay the full surface of the asteroid, and sample the orbit in 5 minute increments. The initial sidereal time of the asteroid was 0 with a rotation rate of 3.3116598 10 ^{4} rad/s.

3.3 Estimated Gravity Field Redistribution

Since the shells, as defined by Gaussians, overlap, the estimation process does not control how a contribution of a particular degree n influences the model. Thus, estimated functions Z_j may deviate from their definition in Eq. 22. To match the estimated function Z_j to that definition, we use projectors onto the subspace of the spherical harmonics.

As mentioned in Section 2.1, the reproducing kernel in Eq. 5 is essentially a projector. However, we now wish to create the discretized form of this projection operator using the quadrature nodes. Let us consider a function f in the subspace P_n and the kernel K_m, where $m \quad n$. By multiplying both sides of Eq. 6 by $^{p}\overline{w_i}$, we have

$$^{p}\overline{w_i} f_m(\ _i) = \sum_{j=1}^{M} (^{p}\overline{w_i} K_m(\ _i \quad \ _j)\ ^{p}\overline{w_j})(^{p}\overline{w_j} f_n(\ _j)); \tag{42}$$

where the number of nodes M is sufficient to discretize Eq. 6 exactly. The matrix K_m, with elements $^{p}\overline{w_i} K_m(\ _i \quad \ _j)\ ^{p}\overline{w_j}$, is a projector on the subspace P_m from the subspace P_n. In other words, this projector provides a means for generating values at the nodes of the lower degree function f_m using values at the same nodes of the higher-degree function f_n. We note that the eigenvalues of the K_m matrix are either 1 or 0. The inclusion of $^{p}\overline{w_j}$ in Eq. 42 is the reason we used these factors in Eq. 38.

We now describe a method for using these projectors to properly distribute the gravity field among the shells of the MRQSphere model. First, we select a shell with index j and associated quadrature nodes at $\ _k$ (usually the last shell estimated), which models the function Z_j of degree n. Next, we evaluate the currently estimated potential $U(\ _k; J = \{j_{min}, \ldots, j\})$ at the nodes of the selected shell j. In this case, $\ $ is the lowest valid radius for the model using only shells j_{min} through j. Applying the projector, we generate the values $^{p}\overline{w_i} U_m(\ _i)$ at each of the quadrature nodes, where $U_m(\ _i)$ refers to the potential of degree m. We perform this operation for each degree $m = 2, \ldots, N \quad 1$. Rearranging Eq. 2 and multiplying by $^{p}\overline{w_i}$, we have

$$\begin{aligned} ^{p}\overline{w_i} V_m(\ _i) &= \Big(^{p}\overline{w_i} U_m(\ _i)\Big) \quad \sum_{p=2}^{m+1} {}^{(p+1)}\Big(^{p}\overline{w_i} V_p(\ _i)\Big)^{\,m+1} \\ &= \Big(\big(^{p}\overline{w_i} U_m(\ _i)\big) \quad \big(^{p}\overline{w_i} U_{m\ 1}(\ _i)\big)\Big)^{\,m+1}. \end{aligned} \tag{43}$$

Thus, after mapping the full estimated gravity potential to the lower degree subspaces, we now have a representation of $V_m(\ _i)$ for $m = 2;:::;N \quad 1$. Using

$$V_m(\ _k) =$$

Fig. 17 Precision of the estimated MRQSphere model with the spherical harmonics model, de ned by the number of common digits between them, with the gure on the right illustrating the distribution of accuracy with radius

curacy of 4 or 5 digits yields a model accurate to just as many digits. The decrease in precision for low altitude points, i.e. points requiring the evaluation of shell 8, is a result of reduced accuracy for the nal shell estimated. If the estimation process had been truncated with shell ve and only points above 4.6 R_E were tested, results demonstrate this downward trend would still be seen. These results have not been provided in the interest of brevity.

Figure 18 provides the relative accuracy of the Laplacian of the estimated model. Unlike the acceleration vector, there is a small radial dependency on the accuracy of the Laplacian, especially as the radius decreases towards 17:22 R_E. Like the idealized model results of Fig. 9, the ability of the Laplacian to satisfy the constraints of potential theory depends on the accuracy of the model. In this case, an MRQSphere accurate to 5 digits yields a Laplacian with a relative accuracy of approximately 10^{-5}.

Figure 19 illustrates the spatial distribution of errors in the estimated MRQSphere model. Errors do not correspond to regions of high gravity variability, but are more coupled with the distribution of measurements over the surface of the asteroid. In Fig. 20, we process observations for shell 8 with large regions deprived of measurements. Peak anomalies on the plot correspond to regions with no observations and have doubled in magnitude. Regions with observations exhibit results mostly comparable to those in Fig. 19. Of course, this is an issue with spherical harmonics gravity model as well. A primary example of this phenomenon is estimation of the lunar gravity eld where little is known about the Moon's far side gravity terms (Konopliv et al, 2001).

In Figure 21, we provide the degree variances of the NEAR15A model, the nominal and estimated MRQSphere models, the di erences between the MRQSphere models and the NEAR15A, and the estimated error in the NEAR15A model. To generate the variances for the nominal MRQSphere model, we evaluate the poten-

Fig. 18 Relative accuracy of the Laplacian ($r^2 U$) of the estimated MRQSphere model when compared to the maximum diagonal element of the variational equation matrix, with the gure on the right illustrates the distribution of signi cant digits with radius

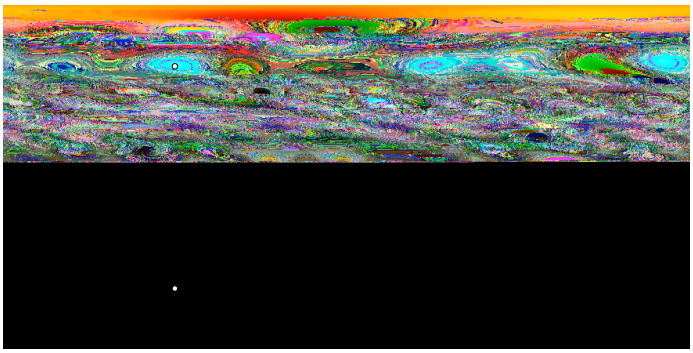

Fig. 19 Gravity anomalies for estimated h=0.425 MRQSphere model at R=2R_E

tial at 2,000 random points with a radial distance of 2 R_E. Given the resulting

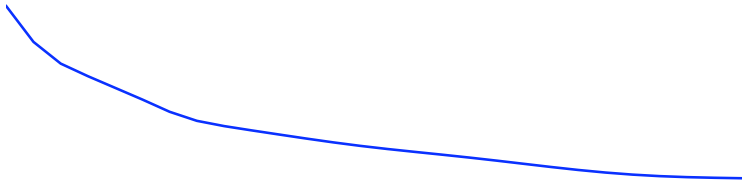

Fig. 22 Summary of 3D RMS position and velocity errors for orbits propagated with the estimated MRQSphere model versus the spherical harmonic model.

term dominates and gravity perturbations attenuate. However, a 1 m 3D RMS error is less than the 5 m orbit determination error for the NEAR mission satellite at comparable altitudes.

4 Conclusions and Future Work

In this paper, we de ned the MRQSphere model and provided its example representing the gravity eld of the asteroid 433 Eros. We used this example to describe performance of the model in the idealized situation. The construction of the MRQSphere model is dependent on several user-de ned tuning parameters, most notably the accuracy of the Gaussian approximation of inverse powers of distance . This approximation allows for the multiresolution representation of the gravity eld and leads to the de nition of the shells to account for its angular variations. Other presented results include the derivation of the acceleration vector and the variational equations within the MRQSphere model.

This paper also demonstrated the estimation capabilities of the MRQSphere gravity representation forectorrepr 8alandy62aohey62rr.s[(In)-416(this)-417of0o account 8ro-ccoui62y62

model was estimated with accuracies comparable to the measurements provided. Like the spherical harmonics model, large regions without measurements yielded a reduced accuracy in the total gravity eld.

The two major goals for future work are: (1) integrating the MRQSphere model with a more traditional orbit determination scheme using a SRIF, and (2) altering the representation for evaluation within the circumscribing sphere. Integration of

with

$$\frac{@K_0(\ )}{@} = 0 \tag{51}$$

$$\frac{@K_1(\ )}{@} = \frac{3}{2}: \tag{52}$$

The resulting acceleration vector, with terms expressed using matrix operations, is

$$\begin{aligned}\mathbf{r} &= r\mathcal{U} \\ &= \frac{}{R}\sum_{j2Z} e^{\ (\ln\ )^2\ {}^2_j=2}\left[\frac{{}^2_j}{r^2}(\ln\ )Z_j(\mathbf{r})\ \mathbf{r} + \frac{@\mathbf{r}}{@\mathbf{r}}\sum_{l=1}^{N} w_l Z_j(\ _l)\frac{@K_N(\ )}{@}\Big|_{\ _l}\right]\end{aligned} \tag{53}$$

where

$$\frac{@\mathbf{r}}{@\mathbf{r}} = \left(\frac{@\mathbf{r}}{@\mathbf{r}}\right)^T = \frac{1}{r}\mathrm{I}$$

Zuber MT, Smith DE, Cheng AF, Garvin JB, Aharonson O, Cole TD, Dunn PJ, Guo T, Lemoine FG, Neumann GA, Rowlands DD, Torrence MH (2000) The shape of 433 Eros from the NEAR-Shoemaker laser range nder. Science 289:2091{2101